High-spin states in even Hg nuclei and rotation alignment in ^{198}Hg

C. Günther, H. Hübel, A. Kleinrahm, D. Mertin, B. Richter,* W. D. Schneider,† and R. Tischler
Institut für Strahlen- und Kernphysik, Universität Bonn, Bonn, West Germany

(Received 16 August 1976)

High-spin states in even Hg isotopes populated in (α,xn) reactions were investigated by in-beam γ-ray and conversion electron spectroscopy. Several new excited states in the ground state band of ^{198}Hg and in the negative parity bands of ^{198,200}Hg were identified. Half-lives of a number of levels in ^{194,196,198}Hg were measured. In particular we obtain $T_{1/2} = 1.38(4)$ and 1.85(16) ns for the 12^+ and 10^+ states in ^{198}Hg, respectively. Intrinsic quadrupole moments Q_0 derived from these data and the $B(E2,0^+ \rightarrow 2^+)$ agree within the limits of error. These data together with the excitation energies of the ground state band are interpreted within the rotation-alignment model.

[NUCLEAR REACTIONS ^{194,196,198}Pt(α,xn), $E=28$, 31, 34, 48 MeV; measured E_γ, I_γ, $\gamma(\theta)$, $\gamma(t)$, $\gamma\gamma$ coin, I_{ce}, ce(t). ^{194,196,198,200}Hg deduced levels, I, π, $T_{1/2}$, ICC, Λ, $B(\Lambda)$. Rotation-alignment model.]

INTRODUCTION

The even Hg isotopes have been investigated over a wide mass range. The level systematics of the ground state bands from ^{184}Hg to ^{204}Hg is shown in Fig. 1 (see Refs. 1–6). The energies of the 2^+ states are almost constant for all isotopes. In contrast to this behavior the energies of the higher-spin states vary strongly with mass number. The light Hg isotopes show well developed rotational level sequences for $I \gtrsim 6$, whereas in the intermediate mass region a compression of the levels around $I = 10$ is observed.

Theoretical investigations predict oblate deformations for the ground states of the even Hg isotopes with $A \geq 184$ (see, e.g., Refs. 7–11). The rotational bands in the light Hg isotopes have been interpreted as resulting from a transition to prolate deformation at higher spins.[9–11] The energy levels of the intermediate mass isotopes have been explained within the framework of the rotation-alignment model[1,5] and the particle-vibration coupling model.[12] Both models can account for the bunching of the energy levels around $I=10$.

In the nucleus ^{198}Hg the levels with $I^\pi = 8^+$, 10^+, and 12^+ are almost degenerate. In the particle-vibration coupling model this degeneracy implies that the wave functions of the three levels contain large two-particle components.[12] One would then expect a retardation of the $E2$ transitions between these states compared with the $2^+ \rightarrow 0^+$ vibrational transition. On the other hand, the rotation-alignment model predicts rotational $B(E2)$ values for all transitions within the ground state band.[13–15]

In this work we report on measurements of the half-lives of the 10^+ and 12^+ states in ^{198}Hg and investigation of high-spin states in ^{198}Hg and ^{200}Hg. In the course of these experiments we have also measured some other half-lives of high-spin states in even Hg isotopes.

EXPERIMENTAL TECHNIQUES

The even isotopes $^{194-200}$Hg have been studied using γ-ray and conversion electron spectroscopy

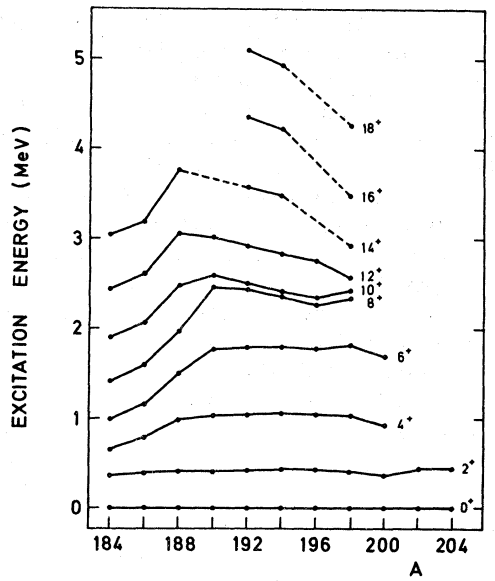

FIG. 1. Level systematics of the ground state bands in even Hg isotopes. The experimental data are taken from Refs. 1–6 and from this work.

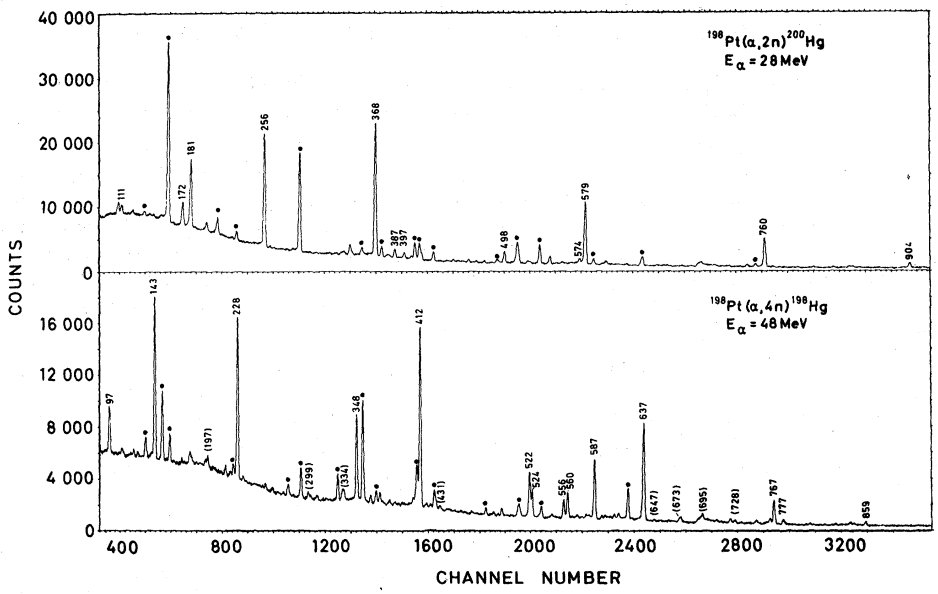

FIG. 2. γ-ray singles spectra measured with the reactions ^{198}Pt(α, $2n$)^{200}Hg and ^{198}Pt(α, $4n$)^{198}Hg at E_α = 28 MeV and 48 MeV, respectively. The spectra were taken with a 26 cm^3 Ge(Li) detector. The lines labeled with energies are assigned to ^{200}Hg and ^{198}Hg. The dots indicate lines which have been identified to belong to neighboring Hg isotopes.

following (α, xn) reactions. The targets were self-supporting metal foils with thicknesses between 700 μg/cm^2 and 5 mg/cm^2. The isotopic composition is given in Table I. The (α, $2n$) reactions were measured at E_α = 28, 31, and 34 MeV and the (α, $4n$) reactions at E_α = 48 MeV.

Singles γ-ray and $\gamma\gamma$-coincidence spectra were recorded with Ge(Li) detectors. Energy and efficiency calibrations were performed with a ^{152}Eu source. Angular distributions of γ rays were measured at eight angles between 35° and 110° with respect to the beam direction for ^{198}Hg and at four angles between 90° and 135° for ^{200}Hg. Conversion electron spectra were measured with an iron-free orange-type β spectrometer. Details of the experimental setup and data analysis are given in Refs. 16 and 17.

Half-life measurements were performed by recording conversion electrons delayed to the beam bursts having a width of $\lesssim$0.5 ns and distances of 47 and 38 ns for the (α, $2n$) and (α, $4n$) reactions, respectively.

TABLE I. Isotopic composition of the targets used in this investigation.

Target	Isotopic abundance A = 194 (%)	A = 195 (%)	A = 196 (%)	A = 198 (%)
^{194}Pt	83.0	13.0	3.5	0.5
^{198}Pt	2.8	4.2	7.0	86.0
^{nat}Pt	32.9	33.8	25.3	7.2

EXPERIMENTAL RESULTS

A. γ-ray and conversion electron measurements in ^{198}Hg and ^{200}Hg

Singles γ-ray spectra measured in beam with the reactions ^{198}Pt(α, $2n$)^{200}Hg and ^{198}Pt(α, $4n$)^{198}Hg are shown in Fig. 2. The energies, γ intensities, and A_2 coefficients of the transitions assigned to ^{200}Hg are summarized in Table II. Our γ intensities contain a small correction for the angular distribution of the γ rays. For some of the lines the intensities increase drastically with energy which indicates that these transitions depopulate high-spin states. The angular distributions were fitted under the assumption of A_4 = 0.

The information on γ transitions assigned to ^{198}Hg including the results of angular distribution measurements is given in Table III. The intensities of the 97, 556, and 637 keV transitions are corrected for small contaminations arising from transitions of similar energy in ^{194}Hg and ^{196}Hg. Our values for the γ intensities and angular distribution coefficients are in good agreement with the results of Proetel, Diamond, and Stephens.[1]

Examples of the $\gamma\gamma$ coincidence spectra for ^{200}Hg and ^{198}Hg are displayed in Figs. 3 and 4, respectively. The coincidence relationships are summarized in Tables IV and V. For a few previously unknown transitions in ^{200}Hg we have measured K-conversion coefficients. The electron and γ spectra were normalized using neighboring transitions of known multipolarity. In Table VI the re-

TABLE II. Energies, γ intensities, and angular distribution coefficients of transitions in ^{200}Hg.

Energy[a] (keV)	γ intensity 24 MeV[b]	28.0 MeV[c]	30.8 MeV[c]	34.4 MeV[c]	Angular distr. coeff. A_2[d]
172.5		6.5	6.4	7.2	−0.02(8)
181.2	3	20	21	20	0.11(3)
255.9	24	48	50	57	−0.49(5)
342.3*		6.3	6.7	5.5	0.16(8)
368.0	100	100	100	100	0.15(2)
387.0		6.2	8.1	7.2	0.25(13)
396.5		3.8	10.5	9.1	0.26(7)
406.9*		12.4	33.1	119	
497.8	<0.5	11.7	16.2	9.0	0.31(8)
573.5		3.5	7.1	9.0	
579.3	80	74	83	87	0.06(6)
759.5	32	61	63	41	0.17(2)
904.2	13	14.3	14.1	3.9	

[a] Energies of previously known transitions taken from Cunnane *et al.* (Ref. 4). Estimated accuracy ±0.2 keV for the new transitions. Transitions marked by an asterisk are not placed into the level scheme.

[b] Taken from Cunnane *et al.* (Ref. 4).

[c] Estimated accuracy ±15% for the measurements at 28 and 31 MeV and the strong lines in the 34 MeV measurement. For the weak lines the accuracy is estimated to be ±50% in the measurement at 34 MeV.

[d] Measured at $E_\alpha = 31$ MeV.

TABLE III. Energies, γ intensities, and angular distribution coefficients of transitions in ^{198}Hg.

E_γ[a] (keV)	I_γ 47 MeV[b]	48 MeV[c]	A_2	A_4
97.3	<7	6.0	0.26(4)	0.04(5)
143.2	20	23	0.31(2)	−0.07(3)
196.5*		2.3		
227.5	38	40	0.29(5)	−0.08(5)
299.0*		2.6		
333.5		4.6		
347.9	35	36	0.30(3)	−0.11(3)
411.8	100	100	0.23(2)	−0.05(2)
431.5*		2.3		
521.6	32	34		
524.1	14	19		
556.1	<23	14	0.43(6)	0.06(7)
560.0		21	0.34(7)	−0.05(8)
587.2	53	51	−0.20(3)	−0.05(3)
636.6	<140	95	0.24(2)	−0.03(2)
646.9*		1.7		
672.5*		3.5		
695.4*		3.9		
728.2*		5.0		
767.3	33	34	0.26(3)	−0.08(4)
776.5		8.2	0.46(9)	0.02(10)
858.6		6.7	0.31(10)	−0.14(12)
935.2*		1.8		
976.7		4.3		
1021.8		3.4		

[a] Estimated accuracy ±0.2 keV for strong lines and ±0.5 keV for weak lines ($I_\gamma \lesssim 5$). Transitions marked by an asterisk are not placed into the level scheme.

[b] From Proetel *et al.* (Ref. 1).

[c] Estimated accuracy ±15%.

sults are compared with theoretical values.[18]

In ^{200}Hg a search for long-lived isomers was performed. In an in-beam measurement γ-ray spectra delayed with respect to the natural beam bursts were recorded. No indication for an isomer in ^{200}Hg with $T_{1/2} \geq 5$ ns was found. In another experiment we irradiated a ^{198}Pt foil with 31 MeV α particles with a total current of 0.5 μAh. We observed the known decay of ^{200}Au→^{200}Hg (Ref. 4), but found no indication for isomeric state with $T_{1/2} \geq 1$ h in ^{200}Hg.

B. Lifetime measurements in ^{194,196,198}Hg

Lifetimes of excited states in ^{194}Hg, ^{196}Hg, and ^{198}Hg were measured by recording conversion electrons after $(\alpha, 4n)$ reactions. In Fig. 5 we show as an example of the conversion electron spectra the L and M lines of the 143 keV $12^+ \rightarrow 10^+$ transition in ^{198}Hg. The time spectra of the 143 keV $12^+ \rightarrow 10^+$ and 522 keV $8^+ \rightarrow 6^+$ transitions in ^{198}Hg are shown in Fig. 6. The solid curves represent the results of fits. For the time spectrum of the 143 keV transition a single exponential function was used. In the case of the 522 keV transition the following function was fitted:

$$N(t) = A\left(\frac{\lambda_1\lambda_2}{\lambda_1 - \lambda_2}\right)(e^{-\lambda_2 t} - e^{-\lambda_1 t}) + B\lambda_2 e^{-\lambda_2 t}.$$

The first part represents the superposition of the half-lives of the 12^+ and 10^+ levels. The second

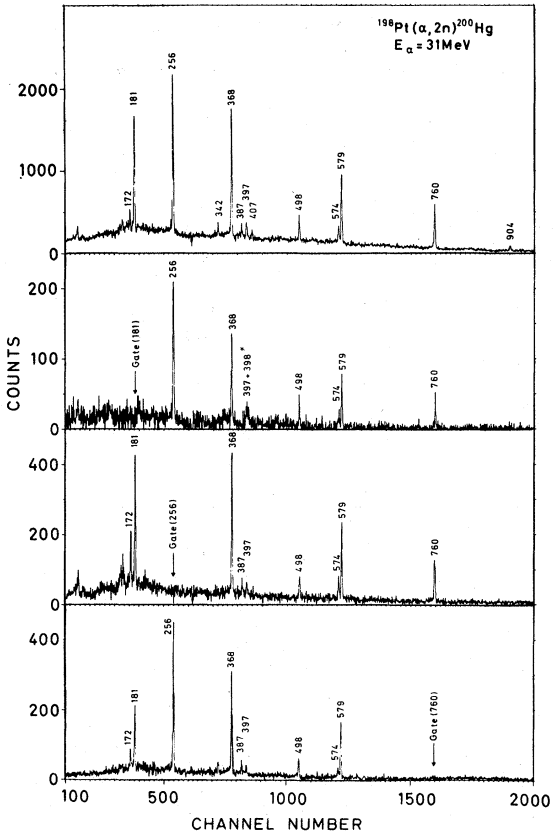

FIG. 3. γ-γ coincidence spectra taken with the reaction ^{198}Pt$(\alpha, 2n)^{200}$Hg at $E_\alpha = 31$ MeV. The upper spectrum is the sum of the coincidence spectra with transitions known from previous work (Ref. 4). The lower three spectra result from coincidences with the 181, 256, and 760 keV transitions. In the coincidence spectrum with the 181 keV line the peak at 398 keV results from 180° backscattering of the 579 keV transition.

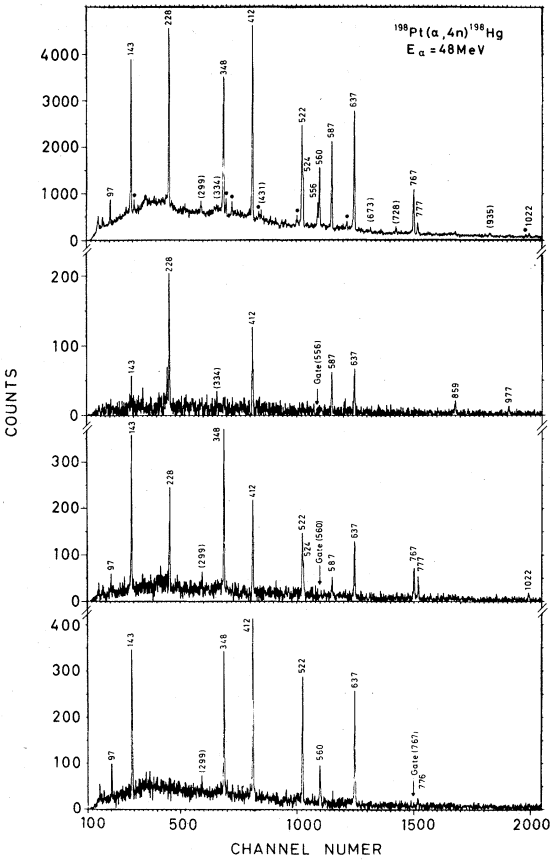

FIG. 4. γ-γ coincidence spectra taken with the reaction ^{198}Pt$(\alpha, 4n)^{198}$Hg at $E_\alpha = 48$ MeV. The upper spectrum is the sum of the coincidence spectra with seven transitions within the ground state band. The lower three spectra result from coincidences with the 556, 560, and 767 keV transitions.

part results from prompt side feeding to the 10^+ state. For the half-life of the 12^+ level (λ_1) the value derived from the 143 keV transition was used. The side feeding to the 10^+ level was varied between 0 and 25%. The position of $t = 0$ was obtained from the prompt contribution to the 522 keV time spectrum. The uncertainties in the side feeding and time zero are included in the error of λ_2. From the time spectrum of the 522 keV line we obtain a value of $(4.1 + 0.8)\%$ for the prompt feeding to the 8^+ state. The results for the half-lives of the 12^+ and 10^+ levels in ^{198}Hg are included in Table VII.

Further examples of our half-life measurements are shown in Figs. 7 and 8. In the case of the 233 keV transition in ^{194}Hg (see Fig. 8) the measured time spectrum consists of two components resulting from prompt feeding of the 9^- level and from delayed feeding via the 10^+ level.[1,5] The half-life

TABLE IV. Summary of coincidence data for ^{200}Hg.

Gate γ ray (keV)	Coincident γ rays (keV)
173	256, 368, 579, 760
181	256, 368, 498, 574, 579, 760
256	173, 181, 368, 387, 397, 498, 574, 579, 760
342	368, 579, 760
368	181, 256, 342, 387, 397, 407, 498, 574, 579, 760
387	173, 256, 368, 579, 760
397	181, 256, 368, 498, 574, 579, 760
407	368, 579
498	181, 256, 368, 396, 574, 579, 760
574	181, 256, 368, 397, 498, 579, 760
579	173, 181, 256, 342, 368, 387, 397, 407, 498 574, 760
760	173, 181, 256, 342, 368, 387, 397, 498 574, 579
904	181, 368, 579

TABLE V. Summary of coincidence data for ^{198}Hg.

Gate γ ray (keV)	Coincident γ rays (keV)
97	143, 348, 412, 522, 560, 637, 767
143	97, 228, 299, 348, 412, 432, 522, 524, 560, 587, 637 728, 767, 777, 935, 1022
197	228, 412, 522, 524, 587, 637
228	143, 197, 334, 348, 412, 524, 556, 560, 587, 637, 647 777, 859, 977
299	143, 348, 412, 522, 524, 560, 587, 637, 767
334	412, 556, 587, 637, 673, 859, 977
348	97, 143, 228, 299, 412, 432, 522, 524, 560, 587, 637 728, 767, 777, 935, 1022
412	97, 143, 197, 228, 299, 334, 348, 522, 524, 556, 560 587, 637, 673, 767, 777, 859, 935, 977, 1022
556	228, 334, 412, 587, 637, 859, 977
560	97, 143, 228, 299, 348, 412, 522, 524, 587, 637, 767, 777, 1022
587	143, 228, 334, 348, 412, 524, 556, 560, 637, 777, 859
637	97, 143, 197, 228, 299, 334, 348, 412, 522, 524, 556, 560, 587, 767, 777, 859
728	97, 143, 228, 348, 412, 522, 524
767	97, 143, 299, 348, 412, 522, 560, 637, 777
777	143, 228, 348, 412, 522, 524, 560, 587, 637, 767
859	228, 334, 412, 556, 587, 637, 977
935	143, 348, 412, 522, 524, 637
977	228, 334, 412, 556, 587, 637, 859
1022	143, 348, 412, 522, 524, 560, 637, 767

of the 9$^-$ state was obtained by fitting an exponential function plus a constant background, approximating the long-lived component to the time spectrum, between $t = 0.6$ and 2.6 ns. The same procedure was applied in the analysis of the time spectrum of the 227 keV line in ^{198}Hg. The results of our half-life measurements are summarized in Table VII. The quoted errors include estimates of the uncertainties in the data analysis. Our value for the 10$^+$ state in ^{194}Hg is in agreement with previous results.[1,5]

TABLE VI. Comparison of experimental and theoretical K-conversion coefficients of transitions in ^{200}Hg.

Transition energy (keV)	$100\times\alpha_k$ Exp.	$E1$	$E2$	$M1$
173	180(40)	8.8	24	142
342	<2	1.7	4.7	22
387	4.5(7)	1.3	3.5	16
396	4.6(7)	1.2	3.3	15
573	0.8(3)	0.6	1.5	5.5

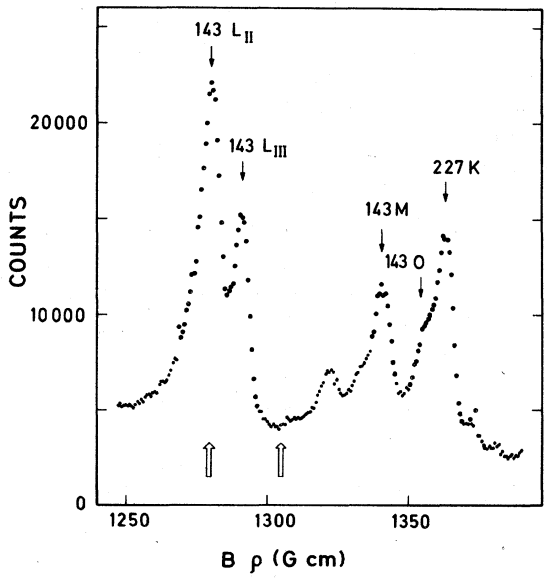

FIG. 5. L- and M-conversion lines of the 143 keV transition in ^{198}Hg. The arrows indicate the spectrometer settings used in the half-life measurement of Fig. 6.

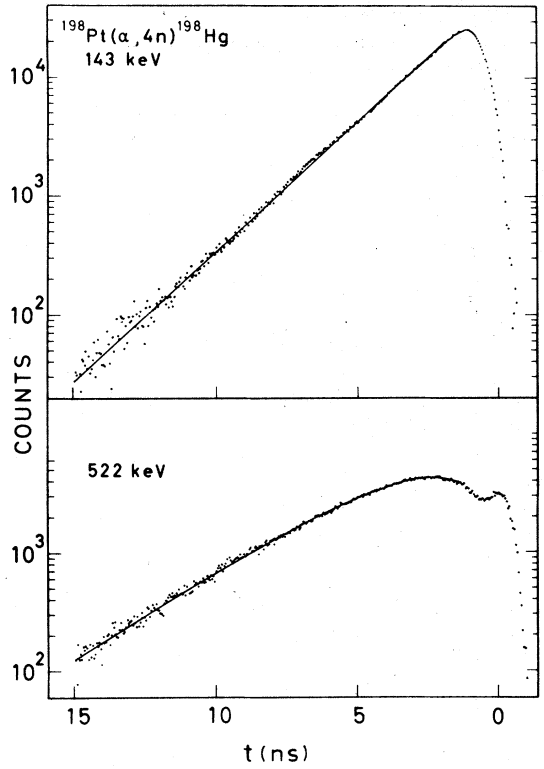

FIG. 6. Time spectra of the 143 keV transition (upper part) and the 522 keV transition (lower part) in ^{198}Hg.

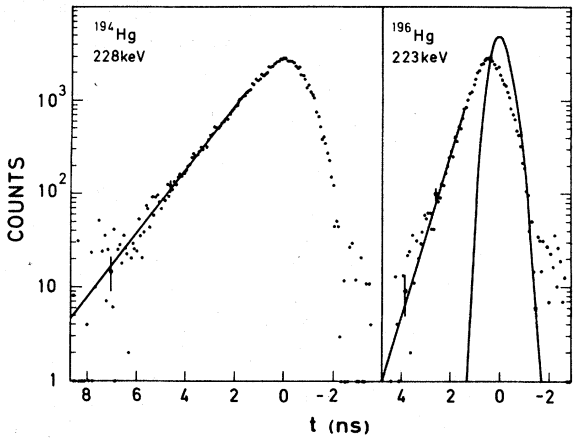

FIG. 7. Time spectra of the 227 keV transition in ^{194}Hg and the 223 keV transition in ^{196}Hg. The results of the fits are indicated in the figure. The solid curve in the right part of the figure is the measured time spectrum of the 348 keV $14^+ \rightarrow 12^+$ transition in ^{198}Hg.

DISCUSSION

A. Level schemes of ^{198}Hg and ^{200}Hg

The level scheme of ^{198}Hg is shown in Fig. 9. The ground state band up to the 14^+ level and the negative parity band up to the 11^- level were known from the work of Proetel *et al.*[1] The 560, 777, and 859 keV lines have angular distributions compatible with stretched $E2$ transitions. The placement of these as well as the 334, 977, and 1022 keV transitions into the decay scheme is derived from the observed γ intensities and $\gamma\gamma$ coincidence relations. The ordering of the levels indicated by dashed lines in Fig. 9 is mainly based on a comparison with the corresponding energy levels found in ^{192,194}Hg (Ref. 5).

In addition to the transitions placed into the decay scheme several weak lines are observed in the $\gamma\gamma$-coincidence spectra (see Table V). The available experimental evidence does not allow a placement of these lines into the decay scheme.

The level scheme of ^{200}Hg is shown in Fig. 10. The levels in the ground state band up to the 6^+ level and the odd spin negative parity band up to the 11^- level were known from previous work (see Ref. 4). The placement of the 173, 387, 397, and

TABLE VII. Half-lives of levels in ^{194}Hg, ^{196}Hg, and ^{198}Hg.

Isotope	Transition[a] (keV)	Level E (keV)	I^π	$T_{1/2}$
^{194}Hg	236.2	3983	16^-	<500 ps
	232.7	2423	10^+	11.6(10) ns
		2143	9^-	291(50) ps
	227.7	2138	8^-	912(30) ps
^{196}Hg	222.9	2064	9^-	355(18) ps
^{198}Hg	347.9	2926	14^+	<120 ps
	143.2	2578	12^+	1.38(4) ns
	521.6	2435	10^+	1.85(16) ns
	227.5	1911	9^-	280(50) ps

[a]In this column the γ transition is given, for which the time spectrum was measured.

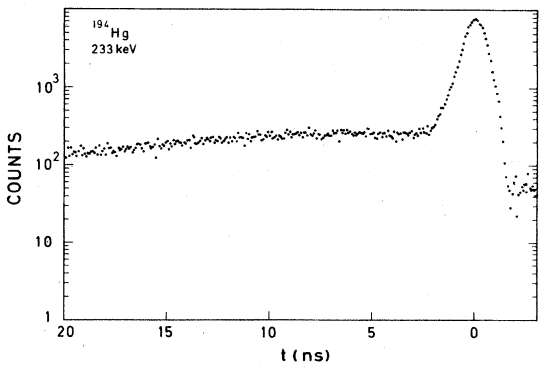

FIG. 8. Time spectrum of the 233 keV transition in ^{194}Hg. The long-lived component results from feeding through the 10^+ state.

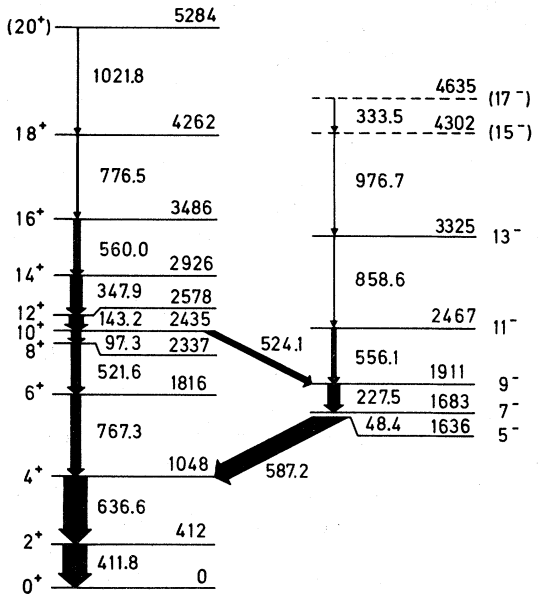

FIG. 9. Level scheme of ^{198}Hg.

574 keV transitions into the level scheme is based on $\gamma\gamma$-coincidence, γ-angular distribution, and conversion electron data. The experimental data on the 173 keV transition allow spins of 6, 7, and 8 for the 2135 keV level. We tentatively adopt spin 8 which can best explain the observed population and decay of this level.[5,20] The K-conversion coefficient of the 574 keV transition favors $E1$ multipolarity (see Table VI). The angular distribution of this line is not accurate enough to allow a spin assignment for the 3612 keV level.

The 342 keV line is in coincidence with the ground state band transitions. Its K-conversion coefficient is only consistent with $E1$ multipolarity. If this transition populates directly the 6^+ state it would define a level at 2049 keV with $I^\pi = 5^-$, 6^-, or 7^-. However, since we only observe the ground state band up to the 6^+ state we cannot exclude that the 342 keV line populates a member of this band with $I > 6$. The 407 keV line results mainly from Coulomb excitation of the first 2^+ level in ^{198}Pt. A further contribution to this line stems from ^{197}Hg (see Ref. 19) as verified in our coincidence measurement. In the coincidence spectra with the 368 and 579 keV transitions a peak at 407 keV appears with approximately the same intensity as the 342 keV line. The data do not allow a reliable placement of the 407 keV line into the level scheme of ^{200}Hg.

B. Reduced transition probabilities

Reduced transition rates for $E2$ transitions in even Hg isotopes are summarized in Table VIII. For the calculation of the partial γ intensities we used theoretical conversion coefficients[18] for which a 3% uncertainty was assumed. For the γ branchings we used $I_\gamma(10^+ \to 8^+)/I_\gamma(10^+ \to 9^-) = (2.4 \pm 0.6) \times 10^{-2}$ for ^{192}Hg (Ref. 5), $(1.73 \pm 0.15) \times 10^{-2}$ for ^{194}Hg (Ref. 1), and $(23.7 \pm 1.7) \times 10^{-2}$ for ^{198}Hg (this work) and $I_\gamma(7^- \to 5^-)/I_\gamma(7^- \to 6^+) = 2.15 \pm 0.13$ for ^{194}Hg (Refs. 5, 21, and this work).

The $B(E2)$ values for transitions within the negative parity bands are strongly enhanced compared with the Weisskopf estimate [$B_w(E2) = 68\ e^2\ \mathrm{fm}^4$].

TABLE VIII. Reduced $E2$ transition rates in even Hg isotopes.

Transition	Isotope	Level half-life (ns)	Transition energy (keV)	Partial γ intensity (%)	$B(E2)$ (e^2 fm^4)	Refs.
$12^+ \to 10^+$	^{198}Hg	1.38(4)	143.2	42.6(12)	2921(117)	This work
$10^+ \to 8^+$	^{190}Hg	24.4(15)	131.8	35.6(7)	208(13)	5, 22
	^{192}Hg	16(3)	60.1	1.01(20)	455(125)	5
	^{194}Hg	11.2(10)	58.9	0.83(4)	594(61)	1, 5, This work
	^{196}Hg	7(1)	97.0	13.5(4)	1267(185)	1
	^{198}Hg	1.85(16)	97.3	8.72(36)	3058(291)	This work
$2^+ \to 0^+$	^{196}Hg				2840(420)	23
	^{198}Hg				1949(114)	24
	^{200}Hg				1758(189)	24
$9^- \to 7^-$	^{194}Hg	0.291(50)	232.7	81.0(5)	2307(396)	This work
	^{196}Hg	0.355(18)	222.9	78.6(5)	2275(115)	This work
	^{198}Hg	0.280(50)	227.5	79.7(5)	2656(474)	This work
	^{200}Hg	1.07(4)	181.2	58.0(8)	1571(63)	25
$7^- \to 5^-$	^{194}Hg	3.75(11)	96.9	11.9(4)	2102(104)	25
	^{196}Hg	5.22(16)	84.0	7.87(24)	2041(87)	25
	^{198}Hg	6.9(2)	48.4	0.589(18)	1935(81)	25

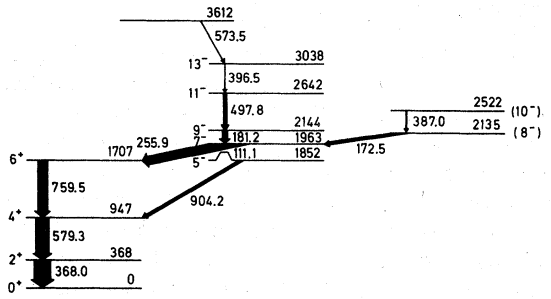

FIG. 10. Level scheme of ^{200}Hg.

This enhancement has been explained by Neergård, Vogel, and Radomski *et al.*[20] within a model of two quasiparticles coupled to an oblate rotor. These authors obtain quantitative agreement for the previously known $B(E2)$ values of the $7^- \rightarrow 5^-$ transitions. However, the experimental $B(E2, 9^- \rightarrow 7^-)$ for ^{200}Hg does not show the predicted strong decrease with increasing neutron number. Our results for the $9^- \rightarrow 7^-$ transitions in $^{194, 196, 198}$Hg confirm this deviation between experimental and theoretical $B(E2)$ values.

For the $10^+ \rightarrow 8^+$ transitions the enhancement increases from $B(E2)/B_w(E2) = 3$ for ^{190}Hg to 46 for ^{198}Hg. For ^{198}Hg the experimental $B(E2)$ values for the $2^+ \rightarrow 0^+$, $10^+ \rightarrow 8^+$, and $12^+ \rightarrow 10^+$ transitions can be compared. Within the framework of the collective model the $B(E2)$ values are given by the relation:

$$B(E2; I\,K = 0 \rightarrow I - 2\,K = 0) = \frac{15}{32\pi} \frac{I(I-1)}{(2I+1)(2I-1)} Q_0^2 .$$

where Q_0 is the intrinsic quadrupole moment. The Q_0 values for the three transitions in ^{198}Hg, which are compared in Table IX, show remarkable agreement. In this table we also give the deformation parameter β_2 derived from the intrinsic quadrupole moment according to the relation[23]:

$$Q_0 = \frac{3}{\sqrt{5\pi}} Z R_0^2 \beta_2 = 2964\, \beta_2 (e\,\mathrm{fm}^2).$$

From the half-life of the 228 keV transition in ^{194}Hg and the $E2/M1$ mixing given by Lieder *et al.*[5] we obtain

$$B(M1,\ 8^- \rightarrow 7^-) = [(1.96 \pm 0.08) \times 10^{-3}]\, \mu_N^2,$$

$$B(E2,\ 8^- \rightarrow 7^-) = 32 \pm 11\, e^2\,\mathrm{fm}^4.$$

These values can be compared to the prediction of Neergård *et al.*[20] who obtain $B(M1,\ 8^- \rightarrow 7^-) = (31 \times 10^{-3})\mu_N^2$ and $B(E2,\ 8^- \rightarrow 7^-) = 730\ e^2\,\mathrm{fm}^4$. Both values are approximately a factor of 20 larger than the experimental results.

TABLE IX. Comparison of $B(E2)$ values for transitions in ^{198}Hg.

Transition	$B(E2)$ ($e^2\,\mathrm{fm}^4$)	$\lvert Q_0 \rvert$ ($e\,\mathrm{fm}^2$)	$\lvert \beta_2 \rvert$
$2^+ \rightarrow 0^+$	1949(114)	313(9)	0.106(3)
$10^+ \rightarrow 8^+$	3058(291)	301(14)	0.102(5)
$12^+ \rightarrow 10^+$	2921(117)	292(6)	0.099(2)

C. Rotation-alignment interpretation of ^{198}Hg

In the previous section it was shown that the known $E2$ transition rates within the ground state band in ^{198}Hg follow the rotational limit. This behavior together with the bunching of the energy levels around $I = 10$ (see Fig. 9) suggests an interpretation of the ground state band in ^{198}Hg in the framework of the rotation-alignment model.[13-15] This model applies to nuclei with moderate deformations such as ^{198}Hg. Furthermore, Nilsson levels with small values of Ω resulting from high j single particle states must lie close to the Fermi surface.

In Fig. 11 the single neutron and proton Nilsson levels around $N = 120$ and $Z = 80$ are shown for oblate deformations. The levels are calculated for ^{199}Hg with the parameters $\chi_n = 0.0636$, $\mu_n = 0.39$, $\chi_p = 0.0620$, and $\mu_p = 0.615$ (see Refs. 26 and 27). The connection between the deformation parameters ϵ and β_2 is discussed in Ref. 27 ($\beta_2 \approx 1.1\epsilon$). As can be seen from Fig. 11 the Nilsson levels resulting from the proton $h_{11/2}$ and neutron $i_{13/2}$ orbits can lead to rotation alignment. However, in $^{198}_{80}\mathrm{Hg}_{118}$ with $\beta_2 = 0.1$ the $(\pi h_{11/2}{}^{-2})$ states are expected at high excitation energies due to the large energy gap between the $d_{3/2}$ and $s_{1/2}$ orbits. On the other hand, the $(\nu i_{13/2}{}^{-2})$ levels are expected at much lower excitation energy for $N = 118$. It can therefore be assumed that in ^{198}Hg the main contribution to the decoupling results from the $(\nu i_{13/2}{}^{-2})$ levels.

In a quantitative calculation it would be necessary to treat the Coriolis coupling of 49 excited levels with spins between 0 and 12. The general behavior of such systems has been studied by Stephens and co-workers.[13-15] Extended calculations including triaxial nuclear shapes and variable moments of inertia were performed by Meyer-ter-Vehn[28] and Toki and Faessler.[29] Recently, Hjorth *et al.*[30] have treated the case of ^{190}Pt in detail. In view of the uncertainties in the parameters entering these calculations we do not present a quantitative description for ^{198}Hg, but instead compare the nuclei ^{190}Pt and ^{198}Hg.

In their decoupling calculations Hjorth *et al.*[30] find that the ground state band in ^{190}Pt can be des-

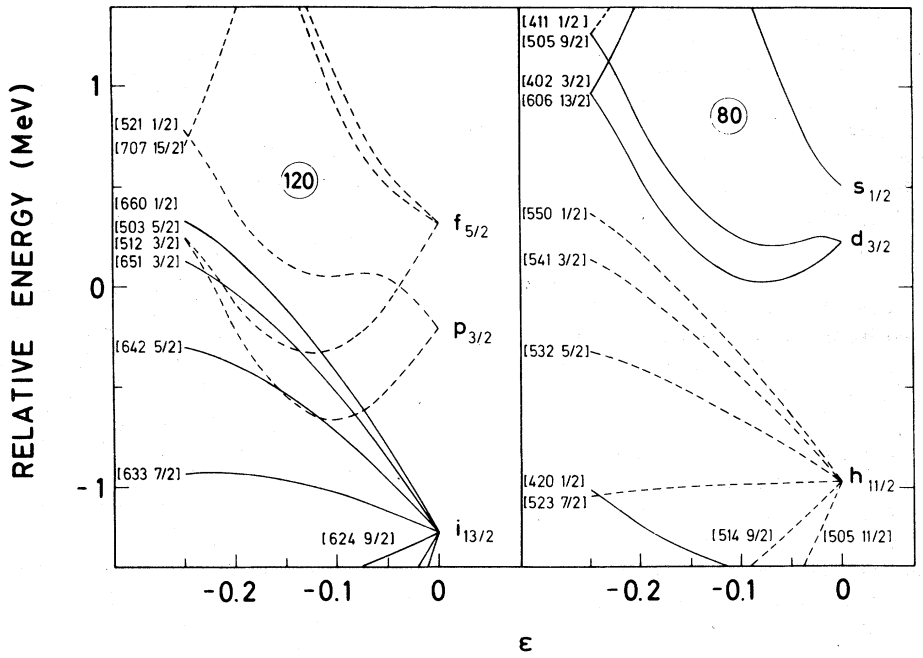

FIG. 11. Single neutron and proton Nilsson levels for ^{199}Hg.

cribed by $(\nu i_{13/2}^{-2})$ aligned states at oblate deformations. Furthermore, they find that for a fixed moment of inertia the results for different deformation parameters are very similar. Therefore one can expect a close similarity between ^{190}Pt and ^{198}Hg, except for the different moments of inertia. This is illustrated in Fig. 12. In the left hand part of the figure the experimental level energies of the ground state bands are compared. In the right hand part the excitation energy is plotted as function of the spin. The dots represent the experimental level energies. The solid curves were obtained by a fit of the energy formula given by the variable moment of inertia (VMI) model[31] to the $I=2$, 4, and 6 states. In the case of ^{190}Pt the experimental energy of the 8^+ level is only 10 keV below the VMI prediction, whereas for ^{198}Hg the experimental 8^+ state lies 357 keV below the VMI curve. The dashed curves for $I \geq 12$ were obtained by VMI model fits for a rotational band with $I=0$, 2, 4, 6 built on the 12^+ level. The bunching of the levels around $I=10$ can be explained with the schematic model of Fig. 12. The different behavior of ^{190}Pt and ^{198}Hg results from the different moments of inertia in these nuclei. The 12^+ levels in the two nuclei appear at approximately the same energy. This is expected since the particle-hole excitations involved are not very sensitive to the deformation.

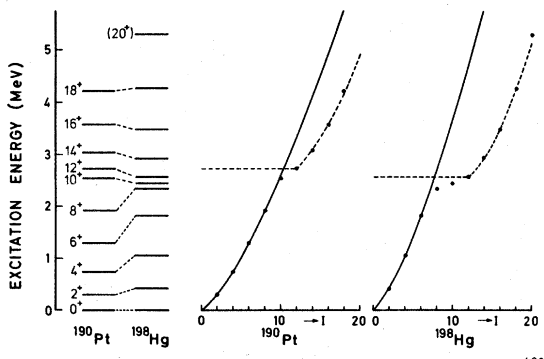

FIG. 12. Comparison of the ground state bands in ^{190}Pt and ^{198}Hg. In the left hand part the experimental level energies are compared. In the right hand part the experimental energies (dots) are compared with a schematic rotation-alignment prediction (solid and dashed lines).

The observed $B(E2)$ values in ^{198}Hg can also be interpreted by the comparison with ^{190}Pt. Hjorth *et al.*[30] find in their calculation a reduction in $B(E2)$ of about 50% for the transition at the intersection between the ground state and rotation-aligned bands. In ^{190}Pt this intersection occurs around the 10^+ level. The calculation gives a retardation of the $12^+ \rightarrow 10^+$ transition whereas all other transitions have nearly the full rotational strength. In ^{198}Hg the intersection of the two bands occurs around the 8^+ level (see Fig. 12). Consequently, the $8^+ \rightarrow 6^+$ transition could be retarded whereas the transitions between the higher-spin states are expected to have rotational strength. This would explain the observed $B(E2)$ values of the $12^+ \rightarrow 10^+$ and $10^+ \rightarrow 8^+$ transitions in ^{198}Hg.

The schematic model described above possibly

also explains the experimental observation that in ^{200}Hg the members of the ground state band with $I \geq 8$ are not observed in the yrast cascade. In this nucleus the rotation-alignment suggested in ^{198}Hg could be hindered by the two additional neutrons filling the last two orbits below the $N=120$ gap (see Fig. 11). In this case the positive parity states with $I \geq 10$ would be much higher in energy than the experimentally known negative parity states.

An alternative description of the ground state bands in the even Hg nuclei within the particle-vibration coupling model has been discussed by Alaga.[12] In this model the 8^+, 10^+, and 12^+ states arise from the $(\pi h_{11/2}^{-2})$ and $(\nu i_{13/2}^{-2})$ configurations and from couplings of quasiparticle states to vibrational excitations. In order to explain the observed enhancement of the $E2$ transitions special mixing of various states and large polarization charges are needed. This seems a rather unnatural explanation compared with the rotation alignment description.

CONCLUSION

The observed values for $B(E2,\ 10^+ \rightarrow 8^+)$ in the even Hg isotopes show an increase from single particle to full rotational strength between ^{190}Hg and ^{198}Hg. This indicates a major change in the structure of these states. In particular the observed data for ^{198}Hg can be explained qualitatively within a schematic model considering a pure $(\nu i_{13/2}^{-2})$ rotation-aligned structure. The different behavior of the lighter Hg isotopes can possibly be explained by an increasing role of the $(\pi h_{11/2}^{-2})$ configuration in the structure of the 8^+ and 10^+ states with decreasing neutron number.[1,5] This may not be unreasonable since in the lighter Hg nuclei the Fermi level for the neutron states is further away from the $\Omega = \frac{1}{2}$ member of the $i_{13/2}$ Nilsson multiplet.

The work was supported financially by the Bundesministerium für Forschung and Technologie of the Federal Republic of Germany.

---

*Permanent address: Kernforschungsanlage Jülich, D-5170 Jülich, West Germany.
†Present address: Universidada Estadual de Campinas, 13.100 Campinas, Brasil.

[1] D. Proetel, R. M. Diamond, and F. S. Stephens, Nucl. Phys. A231, 301 (1974).
[2] D. Proetel, R. M. Diamond, P. Kienle, J. R. Leigh, K. H. Maier, and F. S. Stephens, Phys. Rev. Lett. 31, 896 (1973).
[3] N. Rud, D. Ward, H. R. Andrews, R. L. Graham, and J. S. Geiger, Phys. Rev. Lett. 31, 1421 (1973).
[4] J. C. Cunnane, R. Hochel, S. W. Yates, and P. J. Daly, Nucl. Phys. A196, 593 (1972).
[5] R. M. Lieder, H. Beuscher, W. F. Davidson, A. Neskakis, and C. Mayer-Böricke, Nucl. Phys. A248, 317 (1975).
[6] D. Breitig, R. F. Casten, W. R. Kane, G. W. Cole and J. A. Cizewski, Phys. Rev. C 11, 546 (1975).
[7] A. Faessler, U. Götz, B. Slavov, and T. Ledergerber, Phys. Lett. 39B, 579 (1972).
[8] U. Götz, H. C. Pauli, K. Alder, and K. Junker, Nucl. Phys. A192, 1 (1972).
[9] F. Dickmann and K. Dietrich, Z. Phys. 271, 417 (1974).
[10] S. Frauendorf and V. V. Pashkevich, Phys. Lett. 55B, 365 (1975).
[11] D. Kolb and C. Y. Wong, Nucl. Phys. A245, 205 (1975).
[12] G. Alaga, in *Problems of Vibrational Nuclei*, edited by G. Alaga, V. Paar, and L. Sips (North-Holland, Amsterdam, 1975), p. 344.
[13] F. S. Stephens and R. S. Simon, Nucl. Phys. A183, 257 (1972).
[14] F. S. Stephens, P. Kleinheinz, R. K. Sheline, and R. S. Simon, Nucl. Phys. A222, 235 (1974).
[15] F. S. Stephens, Rev. Mod. Phys. 47, 43 (1975).
[16] M. V. Banaschik, C. Günther, H. Hübel, A. C. Rester, G. Nowicki, and J. J. Pinajian, Nucl. Phys. A222, 459 (1974).
[17] W. D. Schneider and K. H. Gonsior, Nucl. Instrum. Methods 130, 165 (1975).
[18] R. S. Hager and E. C. Seltzer, Nucl. Data A4, 1 (1968).
[19] D. Proetel, D. Benson, Jr., A. Gizon, J. Gizon, M. R. Maier, R. M. Diamond, and F. S. Stephens, Nucl. Phys. A226, 237 (1974).
[20] K. Neergård, P. Vogel, and M. Radomski, Nucl. Phys. A238, 199 (1975); private communication.
[21] R. F. Petry, R. A. Naumann, and J. S. Evans, Phys. Rev. 174, 1441 (1968).
[22] T. Inamura, Y. Tendow, S. Nagamiya, and A. Hashizume, J. Phys. Soc. Jpn. 32, 1163 (1972).
[23] P. H. Stelson and L. Grodzins, Nucl. Data A1, 21 (1965).
[24] H. A. Doubt, J. B. Fechner, K. Hagemeyer, G. J. Kumbartzki, and K.-H. Speidel, Nucl. Phys. A221, 13 (1974).
[25] H. Ton, G. H. Dulfer, J. Brasz, R. Kroondijk, and J. Blok, Nucl. Phys. A153, 129 (1970).
[26] I.-L. Lamm, Nucl. Phys. A125, 504 (1969).
[27] B. Nilsson, Nucl. Phys. A129, 445 (1969).
[28] J. Meyer-ter-Vehn, Nucl. Phys. A249, 141 (1975).
[29] H. Toki and A. Faessler, Nucl. Phys. A253, 231 (1975).
[30] S. A. Hjorth, A. Johnson, Th. Lindblad, L. Funke, P. Kemnitz, and G. Winter, Nucl. Phys. A262, 328 (1976).
[31] M. A. J. Mariscotti, G. Scharff-Goldhaber, and B. Buck, Phys. Rev. 178, 1864 (1969).